Journal of Applied Electrochemistry
https://doi.org/10.1007/s10800-023-02038-z

RESEARCH ARTICLE

# Novel alginate-based binders for silicon–graphite anodes in lithium-ion batteries: effect of binder chemistry on the electrochemical performance

**Alper Güneren[1,2] · Ahmed A. Nada[2,3,4] · Alena Opálková Šišková[4] · Katarína Mosnáčková[2,4] · Angela Kleinová[4] · Jaroslav Mosnáček[2,4] · Zoltán Lenčéš[1]**

Received: 7 June 2023 / Accepted: 18 November 2023


## Abstract

Novel alginate-based binders containing either catechol (d-Alg) or sulfonate (s-Alg) functional groups were developed and characterized to improve the capacity decay performance and better stability of Li-ion batteries. The electrochemical performance of silicon–graphite (Si/Gr) anode with alginate-based binders were compared to the commonly used CMC/SBR binder. The active material in the anodes was the ball-milled Si/Gr (20:80 wt%) powder mixture. A comprehensive electrochemical study was carried out through rate capability test, cycle test, differential capacity analysis (d$Q$/d$V$), and electrochemical impedance spectroscopy (EIS). The functionalized s-Alg binder showed the lowest electrolyte uptake (11.5%) and the highest tensile strength (97 MPa). Anodes with s-Alg exhibited high initial capacity (1250 mAh $g^{-1}$) and improved decay performance (580 mAh $g^{-1}$ at 0.2 C), by ~65% higher compared to CMC/SBR binder. The influence of pH value of s-Alg binder preparation showed that anodes prepared at pH 3 of s-Alg exhibit better performance, reaching 800 and 750 mAh $g^{-1}$ at 0.1 and 0.2 C, respectively, due to the stronger bonding formation and compactness of anode layer which providing low charge transfer and solid electrolyte interface resistance.

### Graphical abstract

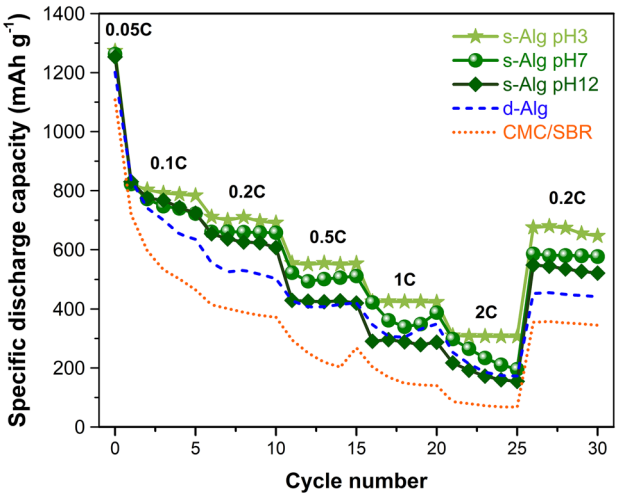


**Keywords** Li-ion batteries · Silicon · Graphite · Anode · Alginate-based binder · Sulfonate

Extended author information available on the last page of the article

Published online: 22 December 2023

## 1 Introduction

Lithium-ion batteries (LIBs) are the premier choice for clean and efficient energy storage for portable devices and electric vehicles with a drawback of low energy density. Silicon (Si)-containing anodes have been reported to provide specific capacities up to 4200 mAh $g^{-1}$ compared to only 372 mAh $g^{-1}$ of graphite anodes [1–5]. Although silicon has an advantage over graphite in terms of capacity, the huge volume change during alloying and de-alloying ($\Delta V > 300\%$) generates large stresses and strains on the silicon particles [1, 2]. This leads to morphological changes of anode, pulverization of silicon, and worse electrical contact. After severe Si particle pulverization by cycling, the freshly exposed surface consumes more electrolyte [3, 4]. The formation of unstable and excessive solid-electrolyte interphase (SEI) increases the internal resistance of the cell and causes the loss of electrical contact [5]. The SEI layers with a thickness between 10 and 35 nm usually crack during each cycle [6], and the exposed fresh electrode surface tends to form a new and thicker SEI layer. All of these structural problems result in capacity fading and limited cycle life [4, 7]. Therefore, polymer binders are necessary to hold together the particulate components in the anode, which is critical for the stable electrochemical performance of the battery.

The main characteristics, which determine the applicability of the best binder system for the high-capacity anodes composed of Si, are as the following: (i) adhesion of the anode to the current collector, (ii) mechanical properties of the binder, and (iii) chemical structure and bonding mechanism with active material. Strong electrode-collector adhesion is required, because it should withstand the high stresses caused by the substantial volumetric change of Si during the charge/discharge processes to maintain the electron flux [8]. The commonly used poly(vinylidene fluoride) (PVDF) in graphite anodes cannot accommodate the huge volume expansion of the silicon anodes due to the low tensile strength and weak van der Waals binding forces [9] owing to the non-functionalized linear chain structure [10]. Such polymer chains tend to slide from the Si surface during cycling, and the connection to the conductive matrix can be broken. Therefore, the traditional binders have been replaced by functional binders, such as carboxymethyl cellulose (CMC), styrene butadiene rubber (SBR), poly(acrylic acid) (PAA), or alginates (Alg) to improve the adhesion [9, 11, 12]. Quite often a mixture of binders is used, e.g., the combination of elastomeric SBR with stiff CMC provides balanced rigidity [12]. CMC/SBR binder mixtures are currently widely used for the anodes in LIBs owing to their good stability in the potential range in which the anodes are operating. However, the cost of these binders is still a significant concern. In addition, it should be noted that the mechanical properties of the binders are also essential for overall anode performance [13]. Not only the poor strength, but even a high rigidity of binder can also be harmful and limit the volume changes, consequently causing crack formation [14]. The cracks can be repaired by self-healing mechanism through hydrogen bonding and the application of self-healing binders can be a good option for Si-based anodes. This is due to their ability to work at room temperature without the need of any stimulating conditions and their mechanical and electrical healing capabilities of cracks formed during battery cycling. Besides improving the physical properties of electrodes, multiplication of the contact points is another route to avoid capacity reduction. An increased number of contacts between the binders and active materials, particularly with Si particles, leads to enhanced binding ability [7] and could be a beneficial strategy to increase the decay performance of LIBs with Si-based anode. For these purposes, alginate has been used as binders in different studies. Gu et al. used alginate and divalent cations to form three-dimensional conductive networks that were able to tolerate the volume change of silicon and enhanced electrochemical performance [15]. Likewise, coordinating alginate molecule chains with different cations was studied [16]. Li et al. provided 3D networks based on alginate and sodium borate that could maintain the structural stability of the silicon anode in long cycle life [17]. Gendensuren et al. investigated a dual-crosslinked alginate with polyacrylamide networks to provide ionic and covalent crosslinkings in the Si anode binder [18]. It is worth noting that the investigated binders are based on the modification or usage of COOH functional groups. However, the effect of increasing the contact points of inexpensive alginate binder by modifying OH groups has not been studied yet.

The main aim of this work is to investigate the effect of the alginate-based binder chemistry by introducing different functional groups promoting multiple hydrogen bonding sites to enhance the binding and the electrochemical performance of silicon–graphite (Si/Gr) anode. Various characterization techniques were performed to analyze the binder systems and their interactions with active materials.

## 2 Experimental

### 2.1 Materials

Sodium alginate (BOS FOOD, Germany), cyanogen bromide (Merck, Czech Republic), dopamine hydrochloride (Sigma-Aldrich, Germany), and ethyl alcohol and acetone (Mikrochem, Slovakia) were used without further purification. Taurine (2-aminoethanesulfonic acid, $H_2NCH_2CH_2SO_3H$,

≥ 99%) was purchased from Merck, Germany. Silicon powder was provided by SicoMill, Vesta Ceramics, Sweden. Graphite was purchased from Imerys Graphite & Carbon, Switzerland, and carbon black (Vulcan PF Carbon Black) from Cabot GmbH, Germany. Citric acid, sodium hydroxide, carboxymethyl cellulose (CMC), ethanol, $LiPF_6$, ethylene carbonate (EC), and ethyl methyl carbonate (EMC) were purchased from Sigma-Aldrich, Germany. Styrene butadiene rubber (SBR) was purchased from Nanografi, Türkiye, and lithium metal (0.75 mm thick ribbon, 99.9% purity) from Alfa Aesar, Germany.

## 2.2 Preparation of active material

Si/Gr active material was prepared by mixing silicon (2 C grade, $d_{50} < 11$ µm, SicoMill) and graphite ($d_{50} < 6$ µm, Imerys Graphite & Carbon) powders in a weight ratio of 20:80 (total 5 gr mixture) using planetary mill (Retsch PM100) in 50-ml tungsten carbide (WC) jar with ø2-mm WC balls applying milling speed of 400 rpm for 12 h. Ethanol (1 g powder / 4 mL ethanol) was used as a milling medium to create a thin oxide layer on the silicon surface with hydroxyl groups.

## 2.3 Characterization of active material

X-ray diffraction (XRD) analysis (Bruker AXS D8 Discover, Cu Kα radiation, 40 mA, 45 kV, $2\theta = 20°$- 80°) was performed to identify the major (C, Si) and minor crystalline residual phases. Scherrer equation was used to calculate the average crystallite size of the milled active material. X-ray photoelectron spectroscopy (XPS) analysis was applied to provide quantitative elemental information from the surface of the powder mixture after ball milling. XPS signals were recorded using a Thermo Scientific K-alpha XPS system (Thermo Fisher Scientific, UK) equipped with a microfocused, monochromatic Al Kα X-ray source (1486.68 eV).

## 2.4 Synthesis of sodium alginate-based binders

Commonly, sodium alginate derivatives are synthesized using coupling reactions consuming the carboxylic groups in the polymer chains to obtain amide covalent bonds. Unlikely, in this work, the hydroxyl groups of the alginate polymer chains are activated by reacting with a mediator, cyanogen bromide, to introduce nitrile functional groups that react with the amino groups of dopamine or taurine. In typical procedure, sodium alginate was dissolved in distilled water (1 g/100 mL) for 2 h at 60 °C until clear solution was obtained. Solution was cooled down to room temperature and pH was adjusted to 10–11. Cyanogen bromide (1.177 g, 2.2 mol) was added to the solution (1-g alginate/100-mL $H_2O$) and left on moderate stirring for 24 h. Dopamine hydrochloride (2.4 g, 2.2 mol) or taurine (2.77 g, 2.2 mol) was dissolved in 10 mL of distilled water and added gradually to the cyanate alginate solution, prepared above, over 2 h. The mixture was stirred at 1000 rpm at room temperature for 3 days and afterward precipitated in acetone and washed thoroughly with acetone several times. Samples were dried on air and stored in the fridge till further use.

The schematic of the synthesis of dopamine alginate (d-Alg) and sulfonated alginate (s-Alg) is shown in Fig. 1.

## 2.5 Characterization of binders

### 2.5.1 FTIR analyses

The FTIR measurements were performed using Nicolet 8700 FTIR spectrometer (Thermo Scientific, UK) having the horizontal single-reflection ATR accessory equipped with a Ge crystal. The spectra were obtained using Globar source, deuterated triglycine sulfate (DTGS) detector and KBr beamsplitter to provide spectra in the 4000–400 $cm^{-1}$ wavenumbers range. Software was setup to scan the background and samples at 64 scans and resolution 4 $cm^{-1}$. A purging time of ca. 15 min with dry air was applied to attain a spectrum without moisture and carbon dioxide impurities [19].

### 2.5.2 Electrolyte uptake

Electrolyte uptake test was conducted to quantify the swelling behavior of the binders. The prepared CMC/SBR, d-Alg, and s-Alg binder films were weighed ($W_{before}$) and immersed into the $LiPF_6$ in EC/EMC (1:1 vol%) electrolyte for 12 h in the glove box under argon atmosphere. Wet samples were weighed after removing the excess electrolyte ($W_{after}$) from the surface. Electrolyte uptake was calculated using the formula: $((W_{after}\text{-}W_{before})/W_{before}) \times 100$ [20]. The measurements were performed three times.

### 2.5.3 Mechanical properties

The tensile tests of alginate samples were performed at room temperature using a Dynamometer Instron 4301 universal tester (Instron Co., Norwood, MA, USA) following the ASTM D638 standard for testing the tensile strength of plastics and other resin materials. Seven testing strips for each composition were cut from the cast films and dipped into EC/EMC (1:1 vol%) solution for 12 h. Dimensions of the tested strip area were 15 × 100 mm with a thickness of approximately 0.04 mm and the gripping distance was 50 mm. A testing rate of 0.1 mm/min was applied until 0.5% deformation was reached, then the rate was increased to 0.5 mm/min. The average values of the tensile strength ($\sigma_t$), elongation/strain at break ($\varepsilon_b$), and Young′s modulus ($E$) were determined from the stress–strain curves using the

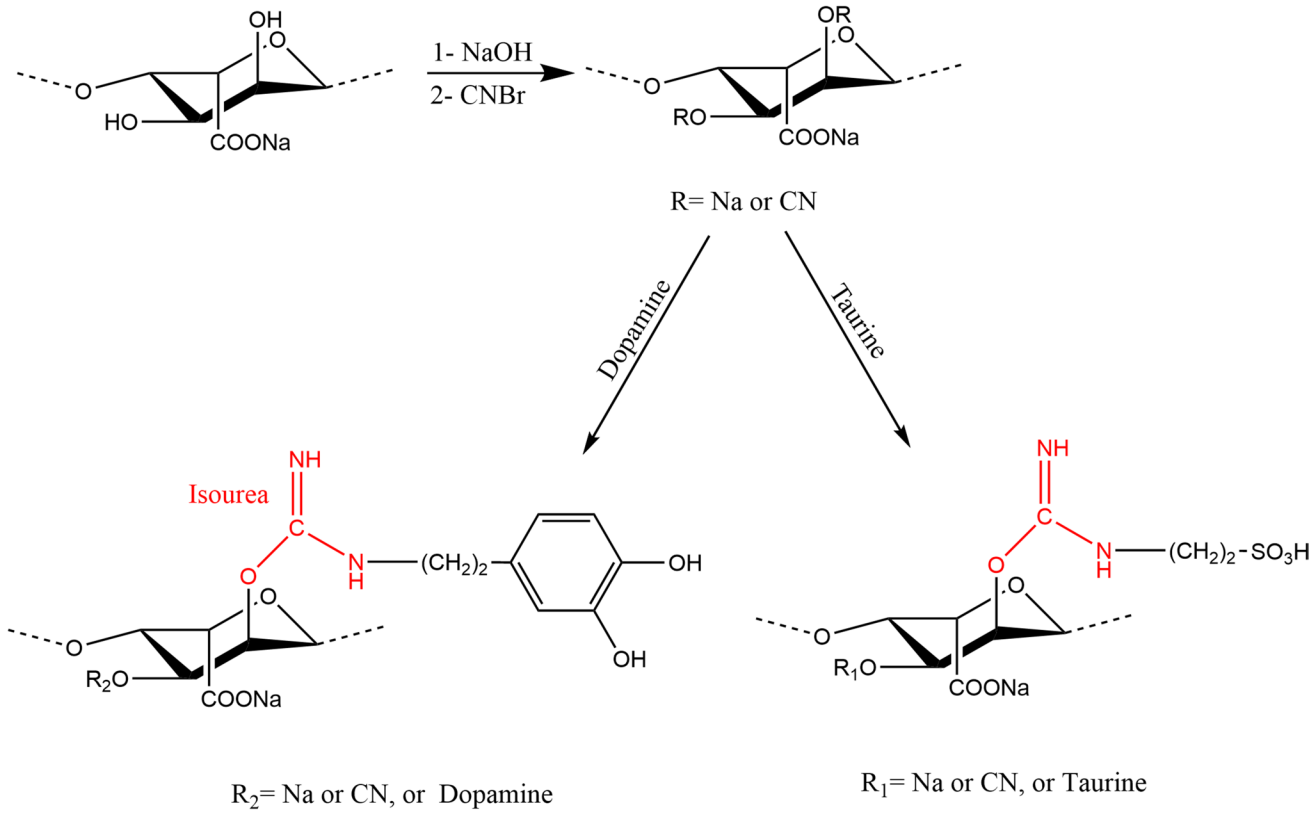


**Fig. 1** Synthesis of sodium alginate derivatives containing catechol (dopamine) or sulfonated (taurine) functional groups

equation $E = \sigma_f/\varepsilon$. The mean values and standard deviations were calculated from 3 specimens for all parameters.

#### 2.5.4 Electrochemical measurements

The milled Si/Gr (20:80 wt%) active material, carbon black (Vulcan PF), and the newly synthesized alginate-based binders (s-Alg and d-Alg) were mixed in deionized water (DI). CMC/SBR binders (1:1) were dissolved in DI:ethanol (30:70) solution. The composition of active material:binder:conductive carbon was adjusted to 80:10:10 in wt%. The anode with only 4-wt% CMC/SBR binder mixture was also prepared to investigate the capacity decay behavior at lower binder content. Apart from the influence of binder content also the influence of pH on the rate performance and cycle life was studied. Therefore, three different s-Alg binder solutions were prepared by dissolving the s-Alg in citric acid, in DI and in the solution of NaOH in DI to adjust the pH value to 3, 7, and 11, respectively. The resulting slurries with ~ 25% solid content were cast onto Cu foil (thickness 6 µm, MTI) using the Zehntner ZAA 2300 automatic tape caster and ZUA 2000.60 universal applicator (Zehntner GmbH Testing Instruments). Films were dried at room temperature for 2 h and afterward in a vacuum dryer at 100 °C for 24 h. Disks with a diameter of 18 mm were punched from the tapes before being transferred into an argon-filled JACOMEX glove box ($O_2$ and $H_2O$ content < 0.5 ppm). The prepared anodes (1 mg $cm^{-2}$ active material mass loading) were dried at 120 °C in a glove box together with PAT-CELL parts and Whatman® glass microfiber (grade GF/A) separators for overnight before assembling. Lithium metal was used as a counter electrode and 100-µl $LiPF_6$ in EC/EMC (50:50 vol%) commercial electrolyte was added. The galvanostatic charge–discharge tests were performed at 25 °C using the 8X-PAT Channel device and EL-CELL software. Initially, the formation cycle with a CCCV procedure between 0.01 and 1.5 V vs. $Li/Li^+$ was applied to all cells using 0.05 C-rate (~ 0.05 mA $cm^{-2}$). For the subsequent cycles, 0.2 C-rate (~ 0.2 mA $cm^{-2}$) was used without a constant voltage step. The rate capability tests were performed at 0.1/0.2/0.5/1/2 C-rates, after the CCCV formation procedure. The differential capacity data ($dQ/dV$) were collected during cycling. Cyclic voltammetry was performed at scanning rates of 0.1 mV $s^{-1}$ between 0 and 1 V vs. $Li/Li^+$. The electrochemical impedance spectroscopy (EIS) measurements were carried out within a frequency range from 100 kHz to 0.1 Hz after rate test and long cycle test. All electrochemical tests were performed at 25 °C.

#### 2.5.5 Morphology of anodes

The cross-sections of the electrodes were investigated using the scanning electron microscope (SEM) JSM Jeol 6610 (JEOL, Tokyo, Japan). The sample morphologies were obtained using 15-kV accelerating voltage [21]. Layer thicknesses were measured by ImageJ software and the standard deviations were calculated from 20 measurements.

## 3 Results and discussion

### 3.1 Characterization of active material

The XRD analysis of active material showed that the major diffraction peaks belong to silicon (28.4°, 47.3°, 56.1°, corresponding to (111), (220), (311) planes) and graphite (26.5°, 42.3°, 44.5°, 54.5°, corresponding to (002), (110), (101), (004) planes), Fig. 2a. A few weak diffraction peaks of tungsten carbide impurity were also observed at 35.6° and 48.3°, respectively. WC contamination could originate from tungsten carbide jar and balls used in the milling process. The average crystallite size of the milled Si/Gr powder was $24 \pm 2$ nm, calculated from the full-width at half-maximum (FWHM) of diffraction peaks using the Scherrer's equation.

The powders were further characterized to check for WC and oxygen contamination using XPS and elemental analyses. The results of XPS analysis showed that there was no signal neither for tungsten (W4f at 32–33 eV) nor for carbide (C1s at 282 eV) [22]. Therefore, the WC content in the milled powders should be very low, either below the detection limit of XPS or randomly distributed WC particles resulting in no detection in the analyzed areas. C1s signal showed a peak at 284.4 eV, which is typical for sp2 carbon (Fig. S1), [23]. Silicon was oxidized only partially and a weak peak of silicon oxide at ~104 eV was observed except of the stronger peak of silicon at 99 eV in Si 2p region (Fig. 2b) [24]. All the used characterization methods of active material confirmed that the powder mixture was only slightly contaminated with oxygen and WC.

### 3.2 Characterization of the alginate-based binders

#### 3.2.1 FTIR analysis

The new binders were synthesized by chemical modification of sodium alginate, an anionic natural polymer, via bonding catechol (1,2-dihydroxybenzene) or sulfonate ($-S(=O)_2-O^-$) functional groups. The functionalization was achieved by chemical modification of the hydroxyl groups in the alginate backbone instead of blocking the carboxylic groups as commonly reported [25]. The functionalized alginate derivatives were obtained via the reaction of primary amines (dopamine and taurine) with the cyanated alginate. The latter, intermediate derivative, was prepared using one-pot procedure for direct transformation of the hydroxyl groups into nitriles using cyanogen bromide. The chemical modifications of alginate by dopamine or taurine were identified by FTIR spectroscopy as shown in Fig. 3.

In the FTIR spectrum of dopamine-modified alginate (d-Alg in Fig. 3a), the peak at 1286 $cm^{-1}$ could be attributed to C−N stretching frequency. The characteristic peaks for dopamine such as O–H of phenol stretching peak at 3210 $cm^{-1}$, alkyl C–H stretching at 2966 $cm^{-1}$, and aromatic C−H stretching at 3050 $cm^{-1}$ could be observed as a broad peak [26]. The strong aromatic C=C stretching peak observed at 1502 $cm^{-1}$ in dopamine was clearly visible with lower intensity at 1528 $cm^{-1}$ in the modified alginate. The

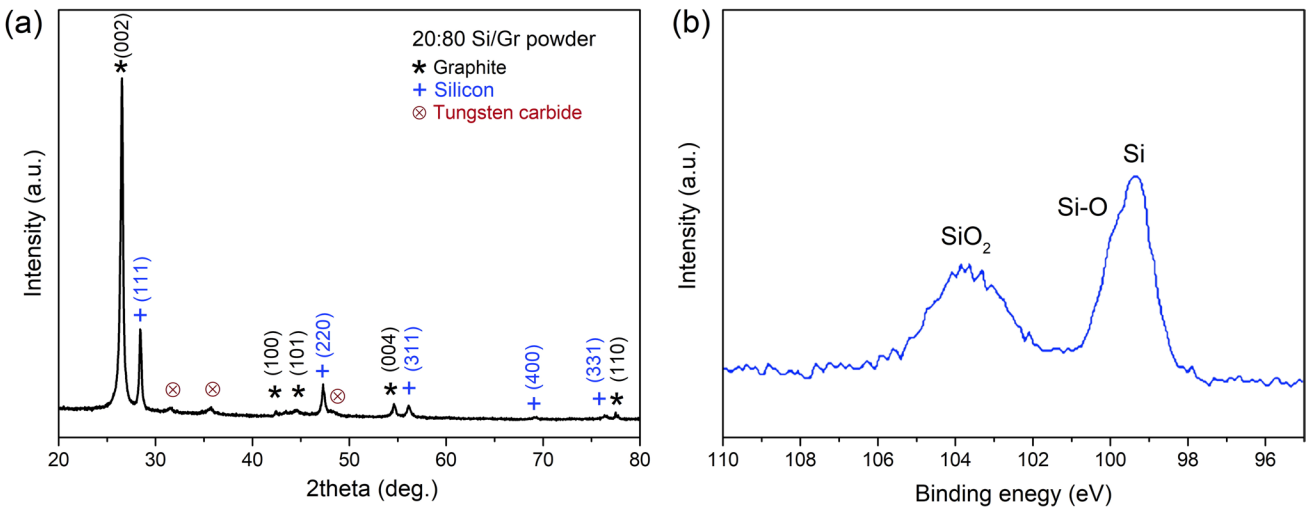


**Fig. 2** XRD pattern (**a**) and Si2p XPS spectrum (**b**) of milled Si/Gr active material

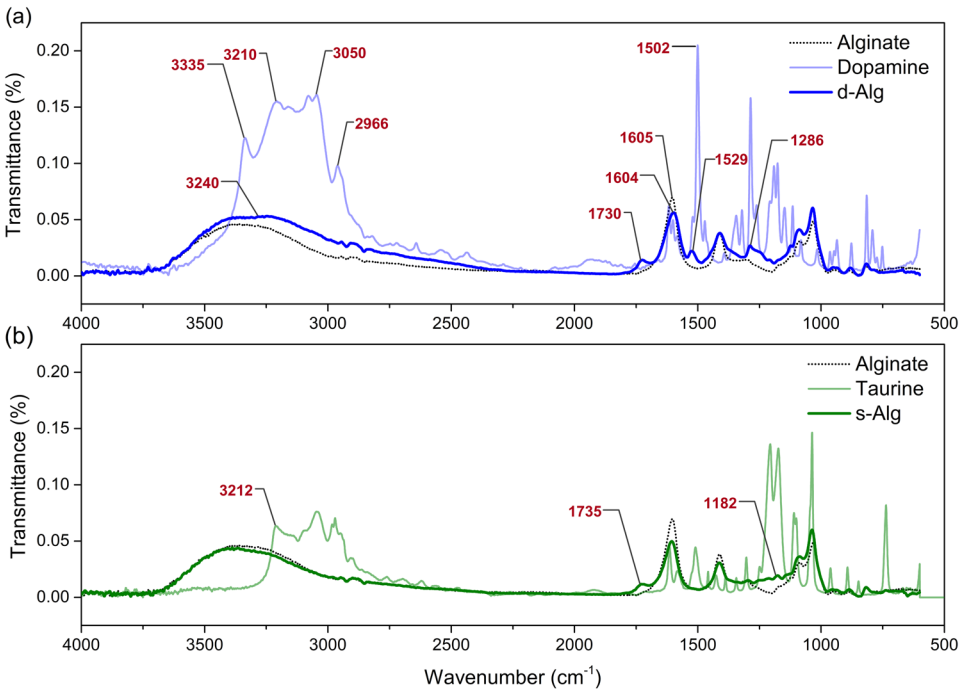


**Fig. 3** The FTIR spectra of pure alginate together with **a** pure dopamine and dopamine alginate (d-Alg) and **b** taurine and sulfonated alginate (s-Alg)

appearance of new peak at 1730 $cm^{-1}$ belonging to the isourea linking group (Alginate-O–C(=NH)–NH-Dopamine) also clearly proved successful modification of the alginate by dopamine [27]. The other characteristic peaks of the alginate observed at 1605 $cm^{-1}$ and 1430 $cm^{-1}$ for C=O stretching did not change after modification of alginate with dopamine (Fig. 3a). However, the peak of the amidine groups, formed from the nucleophilic attack of amines on the nitrile groups [28], could be overlapped at 1604 $cm^{-1}$ with the carbonyl groups.

Similar to previous derivative, the chemical modification of sulfonated alginate (s-Alg in Fig. 3b) was proved by the appearance of new peak in the FTIR spectrum from isourea linking group (Alginate-O–C(=NH)−NH-Taurine) at 1735 $cm^{-1}$.

### 3.2.2 Electrolyte uptake

Electrolyte uptake determines the swelling behavior of the binder, which is essential for the electrode stability during the charging/discharging process when the expansion and shrinkage of Si takes place. It is well known that electrolyte solvation in the binder weakens the molecular interaction strength [14]. The electrolyte uptake in the CMC/SBR binder was up to 39% (Fig. 4), meaning that the functional groups were solvated considerably by $LiPF_6$ in EC/EMC electrolyte solution. Excessive absorption may also represent a high electrolyte consumption, which is one of the main reasons for the low Coulombic efficiency and fast capacity decay together with the low adhesion strength. Furthermore,

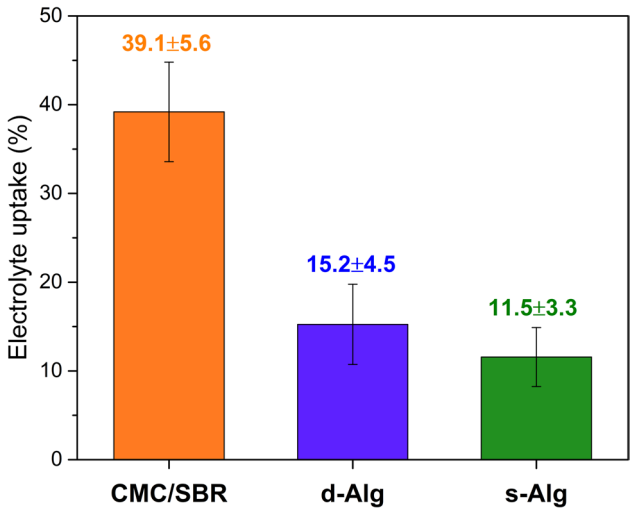


**Fig. 4** Electrolyte uptakes of the CMC/SBR, d-Alg, and s-Alg binder films

swelling of the binders may increase stresses on electrode particle surfaces and cause delamination of both active materials and current collector in perpendicular dimension even before the test [29]. Contrarily, the uptake of the newly synthesized binders was limited and remained at only 15.2% and 11.5% for d-Alg and s-Alg, respectively. This can be attributed to the higher hydrophilicity of the alginate derivatives resulting in a weak electrolyte interaction, thereby, providing a stronger binding, longer stability, and lower delamination between particles.

### 3.2.3 Mechanical properties of binders

Besides electrolyte uptake also the mechanical properties of the binders significantly influence the performance of LIBs. Recent studies confirmed that the stabilization of Si-based anode mainly depends on the tensile strength ($\sigma_t$), Young′s modulus ($E$), elasticity (strain $\varepsilon$), where $\sigma_t = E \bullet \varepsilon$, and adhesion ability of the polymeric binders [30]. Binder should be strong enough to compensate the silicon volume changes, but also it should be able to swell enough to prevent crack formation [14]. Here, important parameter is mechanical properties of binders in wet condition because binders operate in anode in liquid electrolyte medium. The tensile tests (Table 1) revealed that Young′s modulus of s-Alg and d-Alg binders are close to 4 GPa, while for CMC/SBR binder, it is only 0.7 GPa. Moreover, CMC/SBR has the lowest tensile strength of 14.3 ± 5.2 MPa. On the other hand, s-Alg and d-Alg films are relatively stiff, with a higher tensile strength of 97.0 ± 2.6 MPa and 73.0 ± 7.5 MPa, respectively (Fig. 5). According to the results, 98.7% negative correlation was detected between the tensile strength and electrolyte uptake (Table 1), which can be attributed to the weakening of the intermolecular interaction by the electrolyte.

**Table 1** Mechanical properties and electrolyte uptakes of CMC/SBR, d-Alg, and s-Alg binder films

| Binder | $E$ (GPa) | $\sigma_t$ (MPa) | $\varepsilon$ (%) | Electrolyte uptake (%) |
|---|---|---|---|---|
| CMC/SBR | 0.7 ± 0.1 | 14.3 ± 5.2 | 4.6 ± 2.2 | 39.1 ± 5.6 |
| d-Alg | 4.2 ± 0.3 | 73.0 ± 7.5 | 4.3 ± 1.7 | 15.2 ± 4.5 |
| s-Alg | 4.0 ± 0.1 | 97.0 ± 2.6 | 7.4 ± 0.3 | 11.5 ± 3.3 |

## 3.3 Electrochemical properties

### 3.3.1 Influence of binders on the electrochemical performance

The electrochemical performance of all samples was evaluated in half-cell configuration in the potential range of 0.01–1.5 V vs. $Li/Li^+$. The capacity decay performances of the anodes prepared with CMC/SBR, d-Alg, and s-Alg binders were investigated by galvanostatic charge–discharge test at 0.2 C-rate, followed by 0.05 C-rate formation cycle and are shown in Fig. 6. The anode with 4-wt% CMC/SBR binder content showed an initial discharge capacity of 1000 mAh $g^{-1}$, with low initial columbic efficiency (ICE = 63%) and a sharp decay in the first cycles. Generally, the initial capacities are linked to the active material utilization, mainly to silicon in Si/Gr anodes [31]. The results indicate that some of the silicon particles remained electronically isolated even during the first cycles. Moreover, the capacity was barely stabilized after 10 cycles and decreased to 200 mAh $g^{-1}$, which is lower than that of graphite anode [32]. Therefore, lower initial capacity and higher irreversible capacity loss can be explained by insufficient binder ratio, low mechanical properties, and high swelling behavior of the binder [33], resulting in morphological changes, cracking of silicon particles, and pulverization of the anode [4]. Similarly, the sample with 10% CMC/SBR binder showed poor decay performance. However, the initial capacity was relatively higher (1150 mAh $g^{-1}$) than that for the 4% CMC/SBR sample and decreased to 336 mAh $g^{-1}$ after 20 cycles. These results suggest that at least 10-wt% CMC/SBR binder should be used in Si/Gr (20:80)-blended composite anode to ensure

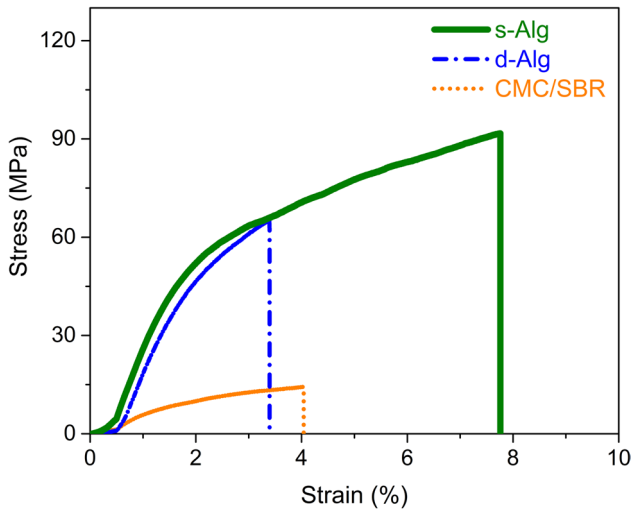


**Fig. 5** Tensile stress/strain curves of the CMC/SBR, d-Alg, and s-Alg binder films

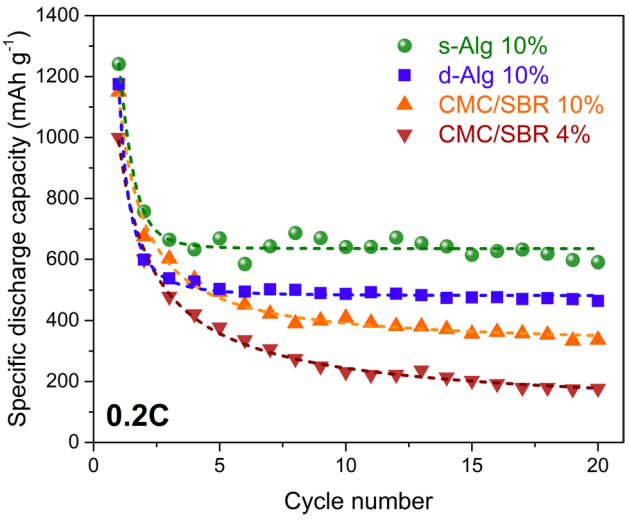


**Fig. 6** Capacity decay performances of the anodes prepared with CMC/SBR, d-Alg, and s-Alg binders at 0.2 C-rate

a sufficient amount of binding with active materials and to avoid further pulverization of Si, which is essential for maintaining a good electrical contact during cycling. In contrast, samples with d-Alg and s-Alg binder exhibited enhanced performance with higher initial capacities, 1175 mAh $g^{-1}$ and 1250 mAh $g^{-1}$, respectively. ICE reached ~ 70% for both anodes. After a few cycles, the capacities became stable on the level of 465 mAh $g^{-1}$ and 590 mAh $g^{-1}$, respectively, up to 20 cycles (Fig. 6). Detailed voltage/time evolution and CE values of all anodes are given in Figs. S2,S3 to provide more detailed data about the charge efficiency of each cycle. These results show that the molecular-level interaction between the binder and the Si surface is one of the most critical factors and the setup of the chemical bonds determines the strength of the Si-based anodes. The OH − groups on the silicon surface and current collector surface interact with the functional groups of the binders via different mechanisms [14], such as weak van der Waals bonds, hydrogen bonding, or covalent bonding. In this study, the functionalized alginate-based binders with higher elastic modulus and relatively high tensile strength have an increased number of hydrogen bonding sites, which provide self-healing properties (Fig. S4) and better long-term integrity of silicon particles [2, 34], contrary to the insufficient bonding with the linear structure of CMC/SBR binder; thus, fitted lines ($R^2_{adj} = 0.99$) showed that anodes with alginate derivatives have stable cycle performance at low C-rate. The sample with s-Alg had better performance because s-Alg has double anionic functional groups on the alginate backbone with more possible hydrogen bonding sites than that of d-Alg. It can be said that the more contact points on a binder provide better electronic network and electrode stability. However, it should be pointed out that the type of functional groups is as vital as the number of binding sites for anode performance because they mainly determine the system's swelling mechanism, mechanical strength, adhesion force, and fatigue behavior during repeated cycles. Poor properties with higher contact points cannot withstand the enormous expansion/shrinkage; thus, decay is inevitable.

Additional investigations at different C-rates (0.1, 0.2, 0.5, 1, and 2 C) were carried out to evaluate the rate capability performance of the binders. Similar to the previous tests, the CC-CV charging method was applied for the formation cycle to fully activate the silicon particles. The C-rate increased gradually from 0.1 to 2 C and returned down to 0.2 C. The results showed that the anode with s-Alg exhibited better performance (725 mAh $g^{-1}$ at 0.1 C) than the d-Alg, particularly at lower current densities, as shown in Fig. 7. The capacities of both branched structure alginate derivatives dropped to the same level after 0.5 C. The sample with linear CMC/SBR binder showed the lowest rate performance in all C-rates. The stabilization of the anode took more cycles, and the capacity decreased to 372 mAh

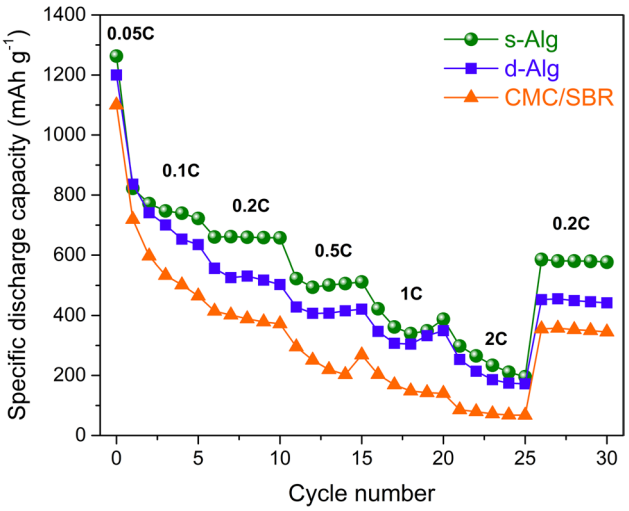


**Fig. 7** Rate performances of the Si/Gr anodes containing CMC/SBR, d-Alg, and s-Alg binders

$g^{-1}$ at 0.2 C and almost disappeared at 2 C for the anode with CMC/SBR binder. Despite the dramatic loss of capacity at 2 C-rate, the capacity could recover to 354 mAh $g^{-1}$ at 0.2 C. On the contrary, the anodes prepared with the newly synthesized s-Alg and d-Alg binders demonstrated high reversibility and the capacities remained at 445 mAh $g^{-1}$ and 580 mAh $g^{-1}$, respectively, at 0.2 C after 30 cycles.

Outputs of the rate test is also used to determine the Peukert's constant which provides numerical analysis of the rate performance of Li-ion batteries using reformulated equation as follows [35]:

$$C = C_o \left( \frac{I}{I_o} \right)^{1-k}, \quad (1)$$

where $k$ is the Peukert's constant, which is unitless, $C$ and $C_o$ are the discharge capacities measured at current densities of I and $I_o$, respectively, and $I/I_o$ stands for charging current rate. When $k = 1$, the discharge capacity remains constant regardless of the applied current. However, if $k > 1$, the discharge capacity decreases with an increase in the applied current. Peukert's constants were calculated as 2.05, 1.48 and 1.40 using min-max C-rates (0.1 C/2 C) [36] for CMC/SBR, d-Alg and s-Alg, respectively. Furthermore, potential impact of current density ratio on $k$ value was also investigated [37] and detailed calculation was given in supplementary data (Table S1, Fig. S5). Decrease in the capacity as the C-rate increases can be explained by several factors, such as active material degradation, incomplete redox reactions, limited ion diffusion rate, or increased polarization. It is also known that capacity loss at higher $k$ value is more serious due to the severe reaction polarization and $k$ is mainly determined by charge transfer resistance ($R_{ct}$) [38]. According to

calculated $k$ values, it can be mentioned that the anodes prepared by newly synthesized Alg binders have lower resistance, hence they provide higher capacity at all C-rates.

Differential capacity (d$Q$/d$V$) data were collected during the rate test to understand the electrochemical activity and degradation behavior of the anodes. In more detail, the first cycles at 0.1 C-rate were investigated, when mainly the anode stabilization and capacity decay take place. The results are shown in Fig. S6. The lithiation of Si/Gr anode appears mainly in two steps regarding to the alloying/de-alloying reactions of silicon and intercalation/deintercalation of graphite. It is known that while graphite intercalation mechanisms are active below 0.2 V, silicon reactions predominantly take place above 0.2 V [39, 40]. In our composition, silicon provides 70% of the total theoretical anode capacity [41], therefore, a higher attention should be paid to the intensities of redox peaks above 0.2 V, which demonstrate the main contribution to the capacity diversity [42]. The d$Q$/d$V$ measurements indicated the SEI formation at ~0.86 V in the first cycle for all samples (Fig. S7). The Si alloying reaction takes place between 0.31 and 0.24 V, followed by a strong peak at 0.1 V, corresponding to a-Si → a-$Li_2Si$ and a-$Li_2Si$ → a-$Li_{3.5}Si$ conversions, respectively. There is a small peak around 0.05 V, representing recrystallization of a-$Li_{3.5}Si$ phase to c-$Li_{3.75}Si$. It should be noted that Si and Gr redox peaks may overlap each other below 0.2 V. The de-alloying reactions occur at higher potentials, specifically at 0.26 V, 0.43 V, and 0.46 V, corresponding to c-$Li_{3.75}Si$ → a-$Li_{3.5}Si$, a-$Li_{3.5}Si$→ a-$Li_2Si$, and a-$Li_2Si$ → a-Si structural transformations, respectively [43, 44]. The graphite intercalation peaks were detected at 0.2 V and below, at about 0.12 and 0.14 V, corresponding to the formation of $Li_xC$. The characteristic alloying peaks of Si became invisible for CMC/SBR binder during the first formation cycles in differential capacity analysis, while the alginate derivative binders show a steady behavior (Figs. S6b,c).

The cyclic voltammetry test of samples after 30 cycles (Fig. 8) also revealed that the silicon redox peaks (alloying between 0.31 and 0.20 V, de-alloying between 0.26 and 0.49 V) are clearly visible in samples with s-Alg binder, while only partially visible in d-Alg sample and faded for anode with CMC/SBR binder system, indicating that there is no more silicon activation. The results showed that even after high currents, the anodes with s-Alg binder maintained a good binding between the silicon particles and conductive matrix due to the increased number of the anionic functional groups, lower interaction with electrolyte, and better mechanical properties (tensile strength).

### 3.3.2 Effect of pH on the electrochemical performance of s-Alg containing electrode

As the anodes with the s-Alg binder exhibited the best results, additional tests were performed to assess the influence of the pH of the s-Alg binder during the preparation process on the electrochemical performance of the anodes were carried out. There are limited studies on the effect of buffer solutions (carboxyl groups) on the capacity retention of Si-based anodes. Mazouzi et al. [45] showed that lower pH (pH ≤ 3) provides covalent bonding through esterification reaction upon drying between the neutralized SiOH/C(O)OH groups and the strong bonding improves the cycle performance. Similarly, Andersen et al. [46] reported the beneficial effect of lower pH on capacity retention. It was also shown that the pH values of slurry during the preparation also affects the electrode integrity due to the progress of acidic catalyzed, exothermic condensation reactions [34]. However, all the above-mentioned studies were performed at lower C-rate (~0.1 C).

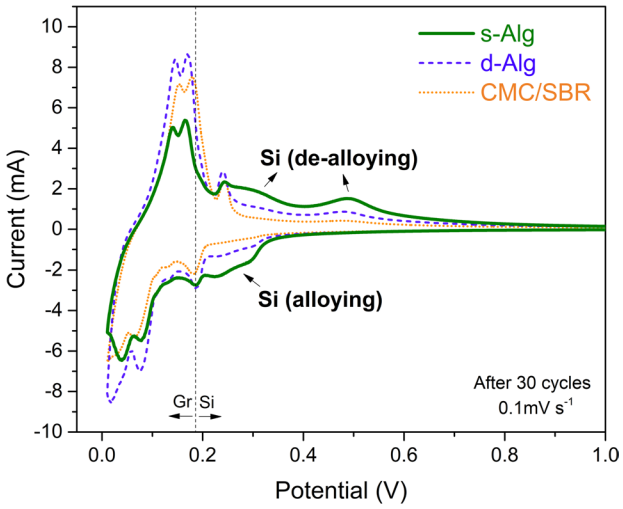


**Fig. 8** Cyclic voltammogram of the Si/Gr anodes containing CMC/SBR, d-Alg, and s-Alg binders

In this work, the effect of pH level on the anionic groups was investigated in the range of 0.05–2 C-rates and the results are shown in Fig. 9. All the anodes had an initial discharge capacity of 1250 mAh $g^{-1}$ with an ICE of ~70%. Anode with s-Alg binder prepared at pH 3 showed 800 mAh $g^{-1}$ capacity at 0.1 C-rate and 650 mAh $g^{-1}$ at 0.2 C-rate after 30 cycles. The capacity at 0.2 C-rate increased by 24%, and 12% compared to the anodes with s-Alg pH12 and s-Alg pH7 binder. The results obtained for 0.1 and 0.2 C-rates are coherent with studies on the influence of pH on the performance of Si-based anodes [38–41]. It is also showed that the acidic medium for anionic binder systems has beneficial contribution to higher current density performance such as 1 and 2 C-rates for limited cycle number.

SEM images in Fig. 10 revealed that stronger hydrogen bonding (with a possibility of formation also strong covalent binding) between the SiOH and $SO_2OH$ groups have been established at pH 3; therefore, the structural integrity

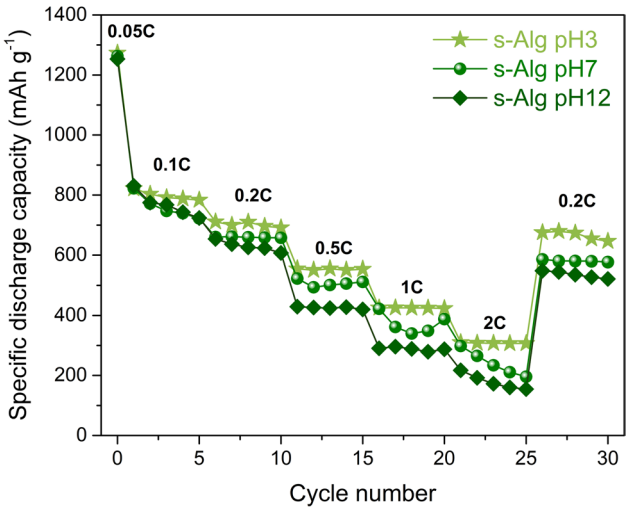


**Fig. 9** Rate performances of the Si/Gr anodes prepared by s-Alg binder dissolved in different pH solutions

is maintained even after 30 cycles. The Zeta potential of the negatively charged active materials and anionic binder is close to zero in an acidic medium [47]. Therefore, neutralization of the surface charges takes place [48]. It can be claimed that the higher obtained capacity at all C-rates was due to the compact layer, a better electrically conductive network, and faster diffusion kinetics. Li-ion diffusion is the rate-limiting factor at higher current rates by contrast with low current reactions, which considerably depends on the electrolyte, SEI, or electrode thickness [49]. It is well known that Li-ion diffusion enhances with shorter ionic pathways [13] and thinner SEI. Here, more potent bonding mechanism prevents extra Si cracks, excessive electrolyte depletion, and further SEI formation. Hence, better integrity and shorter distance for diffusion were provided.

The presence of partially ionized $SiO^-$ and $SO_2O^-$ groups at pH 7 led to moderate hydrogen bonding and allowed limited swelling. Therefore, a slightly higher capacity was obtained for s-Alg pH7 sample at higher currents (0.5–2 C) compared to s-Alg pH12. The full ionization of $SiO^-$ and $SO_2O^-$ groups at pH 12 is unfavorable for high-strength binding because of repelling the negative charges [50] and the structural changes in s-Alg pH12 sample resulted in partial loss of electronical contacts in more porous/thicker layer. The layer thicknesses of samples after 30 cycles were $17.3 \pm 0.9$ µm, $22.2 \pm 2.3$ µm, and $25.2 \pm 2.4$ µm for samples s-Alg pH3, s-Alg pH7, and s-Alg pH12, respectively. (Detachment of layer seen in Fig. 10c is because of handling during SEM sample preparation). The results indicate that the pH value of the binder solution is as essential as the binder type, because it affects the electrode integrity during the cycling, depending on the binding strength. Nevertheless, it should be noticed that all s-Alg binders showed superior performance than d-Alg and CMC/SBR, particularly at low C-rate.

Enhanced capacity can also be explained from a different perspective, as given in Fig. 11. Peak shifting to lower voltage during reduction and higher voltage during oxidation was observed in differential capacity analysis for CMC/SBR, representing higher polarization existence in the cell [51]. All voltage values of redox reaction are given in Table S2. For instance, while a-$Li_2Si$ transformation takes place around 0.3 and 0.24 V for the anodes prepared by all pH level s-Alg binders, the first peak shifted to 0.28 V in CMS/SBR (second reduction peak was not even visible). It is not only for Si alloying, but also the same case for graphite intercalation potential range. Another critical output that can be driven from d$Q$/d$V$ plot is the loss of active materials information from peak intensity. Dramatic differences in peak intensities, especially in the silicon region, were observed in the 30. cycle between anodes similar to cyclic voltammetry results. It is verified that compact anode morphology due to a stronger bonding mechanism in acidic solution (s-Alg pH3) provided higher Si activity after short-term high C-rate exposure.

Electrochemical impedance spectra (EIS) were performed after rate capability (Fig. 12a, b) and long cycle test (Fig. 12c, d) in order to analyze the all results inclusively

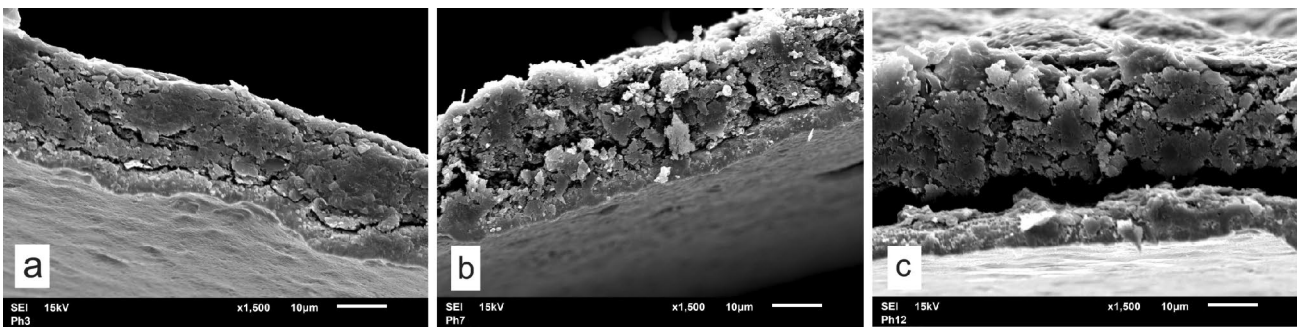


**Fig. 10** Cross-sections of the delithiated anodes prepared by s-Alg binder dissolved in different pH solutions **a** pH 3, **b** pH 7, and **c** pH 12 after rate test

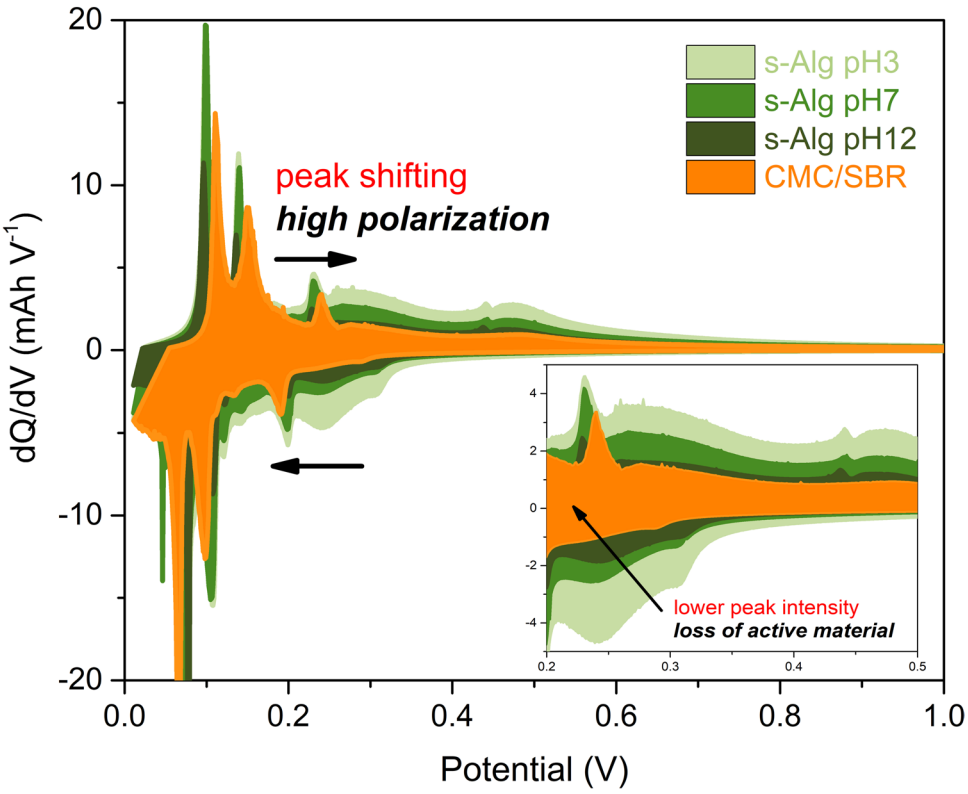


**Fig. 11** Differential capacity analysis of the Si/Gr anodes prepared by CMC/SBR and s-Alg binders dissolved in different pH solutions at 0.2 C-rate at 30th cycle

and summarize them clearly. All measurements were collected after relaxation state. Nyquist plots are composed of solution resistance region $R_e$, two semicircles (one semicircle in high-frequency region representing SEI resistance $R_{SEI}$, one semicircle in middle-frequency region representing charge transfer resistance $R_{ct}$), and Warburg element [52]. Impedance results confirmed that anode prepared by s-Alg pH3 has lowest $R_{ct}$ due to compact layer resulting strong bonding performance, as seen in SEM images. $R_{SEI}$ values for pH3 and pH7 are statistically same but meaningful difference can be seen for pH12 and CMC/SBR system. It proves that binder properties have impact on structural deformations and SEI formation mechanism. Weak binder systems cannot alleviate huge volumetric expansion/shrinkage, cause pulverization of active materials, and form a thicker SEI layer that influences charge transfer kinetic. EIS results are also compatible with Peukert's constants, d$Q$/d$V$ analysis, and the correlation between the redox peaks shifting shown in Fig. 11 and real impedance data were displayed.

Current density has also strong influence on binder decomposition, active material loss, and resistance, as mentioned in [29] and shown our EIS results. Cycle test was carried out to investigate the effect of high C-rate on long-term stability. Figure 13 reveals that faster charging/discharging resulted in excessive deviation of capacity for CMC/SBR due to its poor performance. Sharp decay and recovery can be explained by rearrangement of the active material and conductive network during cycling in the anode which decreases charge transfer resistance. This behavior can be also supported by d$Q$/d$V$ analysis (Fig. S8a). Normally, reduction peaks shift toward lower, while oxidation peaks shift to higher voltage in repeated cycles depending on increased resistance as expected and explained in Figs. 11 and 12. Surprisingly here, d$Q$/d$V$ plots revealed that redox peaks have lower lithiation voltage in the first high-C-rate cycle than 50 and 100 cycles for CMC/SBR anode. High polarization caused non-completed intercalation ($LiC_{12}$ to $LiC_6$) and deintercalation ($LiC_6$ to $LiC_{12}$) reactions in the beginning of 1 C test. Although some recovery was provided later on with the help of better reaction kinetics, no silicon activation was observed during test because of unfavorable properties of the CMC/SBR binder. It should be also noted that redox peak positions were notably different comparing to anode prepared by s-Alg binders, so it means overall resistance of the system was higher. Moreover, electrochemical impedance test results confirmed that $R_{SEI}$ and $R_{ct}$ values almost doubled at 100. cycle. Thus, capacity was recorded quite low throughout the cycle life test. On the other hand, systematic decrease in capacity can be seen for s-Alg pH3, pH7, and pH12. Both peak shifting and decreasing of peak intensities (especially in Si region) were noticed in d$Q$/d$V$ plots (Fig. S8b,c,d). In comparison with CMC/SBR, decay occurred gradually with the help of stronger binder performance and better volumetric compensation.

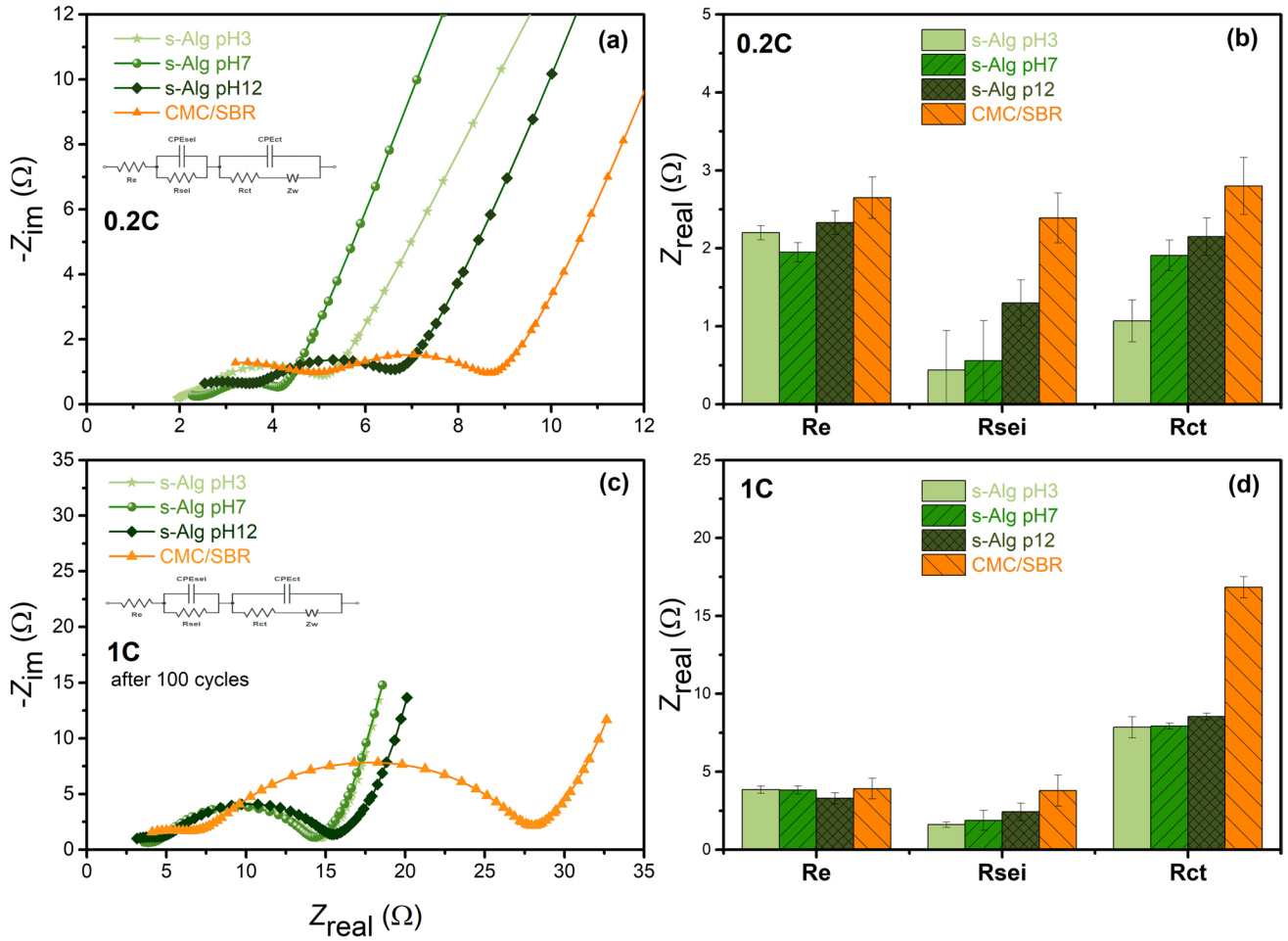


**Fig. 12** Nyquist plots (**a**, **c**) and impedance values (**b**, **d**) of the Si/Gr anodes prepared by CMC/SBR and s-Alg binders dissolved in different pH solutions after rate capability test

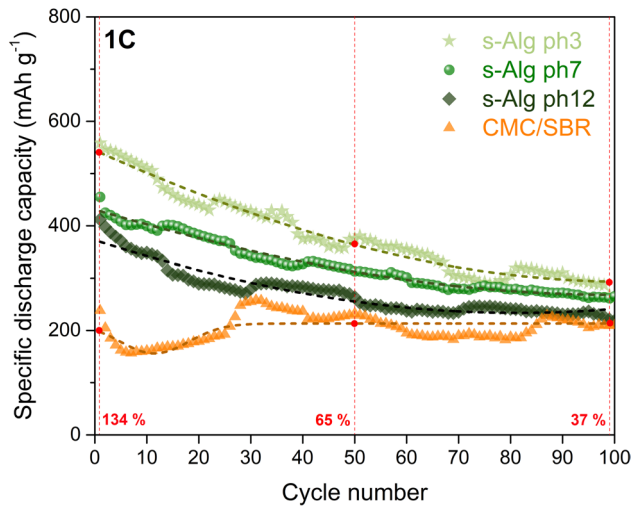


**Fig. 13** Long cycle performance of the Si/Gr anodes at 1 C-rate

Even if s-Alg has stable performance at 0.2 C-rate (Fig. 6), results indicate that just binder performance is not enough to keep cell integrity longer at drastic charging conditions (1 C-rate). Nevertheless, s-Alg pH3 exhibited 400 mAh $g^{-1}$ at 50th cycle and 265 mAh $g^{-1}$ at 100th cycle, respectively (65% and 37% higher than CMC/SBR) due to lower overall resistance and leastwise partially silicon activation. On the other hand, extra effort should be made to improve cycling performance and obtain better stability at higher C-rates for longer term. In addition, electrolyte and binder systems can be improved together to achieve superior performance.

## 4 Conclusion

In this study, the low-contaminated Si/Gr active material (20:80 wt%) was prepared from cheap starting powders via optimized ball milling conditions in WC pot and balls. An innovative water-soluble, eco-friendly functionalized alginate-based binders were developed for high-performance

anode in LIBs. The results showed that the binder structures, mechanical properties, and the number of possible connection points with silicon particles have a strong influence on the obtained capacity, SEI stabilization, and decay performance of the anode. Sulfonated alginate (s-Alg), which has lowest electrolyte interaction and relatively good tensile strength, exhibited strong and sustainable binding ability with Si surface and current collector due to its low hydrophilicity and higher number of hydrogen bonding sites. Anode with s-Alg binder provided better decay performance and higher discharge capacity with lower Peukert's constant value ($k = 1.40$), particularly at lower C-rates (725 mAh $g^{-1}$ at 0.1 C) where the electronic conduction is a limiting factor. The investigation of the pH of the alginate-based binder solution on specific capacity showed an enhanced performance for s-Alg binder solution at lower pH values, close to 800 mAh $g^{-1}$ at 0.1 C due to stronger intermolecular interaction of neutralized OH-SiO groups. Polarization and loss of active material phenomenon were also shown using d$Q$/d$V$ plots and a good correlation was built with electrochemical impedance spectroscopy data. In addition, it was seen that the binder system is also effective in SEI formation and passivation mechanism by providing structural integrity. Lower SEI and charge transfer resistance were obtained with the s-Alg binder. Overall resistance dramatically increased with insufficient CMC/SBR binder after repeated cycles. According to all results, it can be concluded that the binder type and pH level of the binder solution has an apparent effect on the electrochemical performance. The novel water-soluble s-Alg binder offers advantages for Si/Gr-based anodes in LIBs.

**Supplementary Information** The online version contains supplementary material available at https://doi.org/10.1007/s10800-023-02038-z.

**Acknowledgements** This work was performed during the implementation of the project Building-up Center for Advanced Materials Application of the Slovak Academy of Sciences, ITMS project code 313021T081 supported by the Integrated Infrastructure Operational Program funded by the ERDF. The authors thank SRDA grant agency for support through projects APVV-19-0338 and APVV-19-0461 and grant agency VEGA through projects VEGA 2/0167/22 and VEGA 2/0137/23. The XPS measurements carried out by Dr. M. Mičušík are highly appreciated.

**Author contributions** AG contributed to Conceptualization, Methodology, Investigation (Electrochemical analysis), and Writing of the original draft. AAN contributed to Conceptualization, Methodology, Investigation, and Writing of the original draft. AOŠ contributed to Investigation (SEM). KM contributed to Investigation and Validation (mechanical properties). AK contributed to Investigation and Validation (Infrared spectroscopy). JM contributed to Writing, reviewing, & editing of the manuscript, Supervision, and Funding acquisition, ZL contributed to Writing, reviewing, & editing of the manuscript, Supervision, and Funding acquisition.

**Funding** Open access funding provided by The Ministry of Education, Science, Research and Sport of the Slovak Republic in cooperation with Centre for Scientific and Technical Information of the Slovak Republic.

**Data availability** Data will be available on request.

## Declarations

**Competing interest** The authors declare that they have no known competing financial interests or personal relationships that could have appeared to influence the work reported in this paper.



## References

1. Casimir A, Zhang H, Ogoke O, Amine JC, Lu J, Wu G (2016) Silicon-based anodes for lithium-ion batteries: effectiveness of materials synthesis and electrode preparation. Nano Energy 27:359–376. https://doi.org/10.1016/j.nanoen.2016.07.023
2. Wei L, Chen C, Hou Z, Wei H (2016) Poly (acrylic acid sodium) grafted carboxymethyl cellulose as a high performance polymer binder for silicon anode in lithium ion batteries. Sci Rep 6:1–8. https://doi.org/10.1038/srep19583
3. Qi Y, Wang G, Li S, Liu T, Qiu J, Li H (2020) Recent progress of structural designs of silicon for performance-enhanced lithium-ion batteries. Chem Eng J 397:125380. https://doi.org/10.1016/j.cej.2020.125380
4. Wetjen M, Solchenbach S, Pritzl D, Hou J, Tileli V, Gasteiger HA (2018) Morphological changes of silicon nanoparticles and the influence of cutoff potentials in silicon-graphite electrodes. J Electrochem Soc 165:A1503–A1514. https://doi.org/10.1149/2.1261807jes
5. Terranova ML, Orlanducci S, Tamburri E, Guglielmotti V, Rossi M (2014) Si/C hybrid nanostructures for Li-ion anodes: an overview. J Power Sources 246:167–177. https://doi.org/10.1016/j.jpowsour.2013.07.065
6. Pereira DJ, Weidner JW, Garrick TR (2019) The Effect of volume change on the accessible capacities of porous silicon-graphite composite anodes. J Electrochem Soc 166:A1251–A1256. https://doi.org/10.1149/2.1211906jes
7. Jin Y, Zhu B, Lu Z, Liu N, Zhu J (2017) Challenges and recent progress in the development of Si anodes for lithium-ion Battery. Adv Energy Mater 7:1–17. https://doi.org/10.1002/aenm.201700715
8. Gendensuren B, He C, Oh ES (2020) Sulfonation of alginate grafted with polyacrylamide as a potential binder for high-capacity Si/C anodes. RSC Adv 10:37898–37904. https://doi.org/10.1039/d0ra07557d

9. Chen H, Wu Z, Su Z, Chen S, Yan C, Al-Mamun M, Tang Y, Zhang S (2021) A mechanically robust self-healing binder for silicon anode in lithium ion batteries. Nano Energy 81:105654. https://doi.org/10.1016/j.nanoen.2020.105654
10. Liu Z, Han S, Xu C, Luo Y, Peng N, Qin C, Zhou M, Wang W, Chen L, Okada S (2016) In situ crosslinked PVA-PEI polymer binder for long-cycle silicon anodes in Li-ion batteries. RSC Adv 6:68371–68378. https://doi.org/10.1039/c6ra12232a
11. Shen X, Tian Z, Fan R, Shao L, Zhang D, Cao G, Kou L, Bai Y (2018) Research progress on silicon/carbon composite anode materials for lithium-ion Battery. J Energy Chem 27:1067–1090. https://doi.org/10.1016/j.jechem.2017.12.012
12. Hwang C, Joo S, Kang NR, Lee U, Kim TH, Jeon Y, Kim J, Kim YJ, Kim JY, Kwak SK, Song HK (2015) Breathing silicon anodes for durable high-power operations. Sci Rep 5:1–10. https://doi.org/10.1038/srep14433
13. Yoon DE, Hwang C, Kang NR, Lee U, Ahn D, Kim JY, Song HK (2016) Dependency of electrochemical performances of silicon lithium-ion batteries on glycosidic linkages of polysaccharide binders. ACS Appl Mater Interfaces 8:4042–4047. https://doi.org/10.1021/acsami.5b11408
14. Lee SY, Choi Y, Kwon SH, Bae JS, Duck E, Jeong (2019) Cracking resistance and electrochemical performance of silicon anode on binders with different mechanical characteristics. J Ind Eng Chem 74:216–222. https://doi.org/10.1016/j.jiec.2019.03.009
15. Gu Y, Yang S, Zhu G, Yuan Y, Qu Q, Wang Y, Zheng H (2018) The effects of cross-linking cations on the electrochemical behavior of silicon anodes with alginate binder. Electrochim Acta 269:405–414. https://doi.org/10.1016/j.electacta.2018.02.168
16. Wu ZY, Deng L, Li JT, Sen Huang Q, Lu YQ, Liu J, Zhang T, Huang L, Sun SG (2017) Multiple hydrogel alginate binders for Si anodes of lithium-ion Battery. Electrochim Acta 245:371–378. https://doi.org/10.1016/j.electacta.2017.05.094
17. Li J, Hu X, Zhao H, Ren Y, Huang X (2022) Cross-linked sodium alginate-sodium borate hybrid binders for high-capacity silicon anodes in lithium-ion batteries. Langmuir 38:402–410. https://doi.org/10.1021/acs.langmuir.1c02751
18. Gendensuren B, Oh ES (2018) Dual-crosslinked network binder of alginate with polyacrylamide for silicon/graphite anodes of lithium ion Battery. J Power Sources 384:379–386. https://doi.org/10.1016/j.jpowsour.2018.03.009
19. Skoog DADA, Holler FJJ, Crouch SRSR (2006). An introduction to infrared spectrometry, 6th edn. Thomson Brooks/Cole, Pacific Grove
20. Nam J, Kim E, Kim RKKY, Kim TH (2020) A conductive self healing polymeric binder using hydrogen bonding for Si anodes in lithium ion batteries. Sci Rep 10:1–12. https://doi.org/10.1038/s41598-020-71625-3
21. Verreck G, Chun I, Peeters J, Rosenblatt J, Brewster ME (2003) Preparation and characterization of nanofibers containing amorphous drug dispersions generated by electrostatic spinning. Pharm Res 20:810–817. https://doi.org/10.1023/A:1023450006281
22. Rodella CB, Barrett DH, Moya SF, Figueroa SJA, Pimenta MTB, Curvelo AAS, Silva VTD (2015) Physical and chemical studies of tungsten carbide catalysts: effects of Ni promotion and sulphonated carbon. RSC Adv 5:23874–23885. https://doi.org/10.1039/c5ra03252k
23. Blyth RIR, Buqa H, Netzer FP, Ramsey MG, Besenhard JO, Golob P, Winter M (2000) XPS studies of graphite electrode materials for lithium ion batteries. Appl Surf Sci 167:99–106. https://doi.org/10.1016/S0169-4332(00)00525-0
24. Jensen DS, Kanyal SS, Madaan N, Vail MA, Dadson AE, Engelhard MH, Linford MR (2013) Silicon (100)/$SiO_2$ by XPS. Surf Sci Spectra 20:36–42. https://doi.org/10.1116/11.20121101
25. Wang X, Jiang Z, Shi J, Zhang C, Zhang W, Wu H (2013) Dopamine-modified alginate beads reinforced by cross-linking via titanium coordination or self-polymerization and its application in enzyme immobilization. Ind Eng Chem Res 52:14828–14836. https://doi.org/10.1021/ie401239e
26. Thakur A, Ranote S, Kumar D, Bhardwaj KK, Gupta R, Chauhan GS (2018) Synthesis of a PEGylated dopamine ester with enhanced antibacterial and antifungal activity. ACS Omega 3:7925–7933. https://doi.org/10.1021/acsomega.8b01099
27. Mlčochová P, Bystrický S, Steiner B, Machová E, Kooš M, Velebný V, Krčmář M (2006) Synthesis and characterization of new biodegradable hyaluronan alkyl derivatives. Biopolymers 82:74–79. https://doi.org/10.1002/bip.20461
28. Ikawa T, Fujita Y, Mizusaki T, Betsuin S, Takamatsu H, Maegawa T, Monguchi Y, Sajiki H (2012) Selective N-alkylation of amines using nitriles under hydrogenation conditions: facile synthesis of secondary and tertiary amines. Org Biomol Chem 10:293–304. https://doi.org/10.1039/c1ob06303k
29. Foster JM, Huang X, Jiang M, Chapman SJ, Protas B, Richardson G (2017) Causes of binder damage in porous Battery electrodes and strategies to prevent it. J Power Sources 350:140–151. https://doi.org/10.1016/j.jpowsour.2017.03.035
30. Tang R, Ma L, Zhang Y, Zheng X, Shi Y, Zeng X, Wang X, Wei L (2020) A Flexible and conductive binder with strong adhesion for high performance silicon-based lithium-ion battery anode. ChemElectroChem 7:1992–2000. https://doi.org/10.1002/celc.201902152
31. Ruther RE, Hays KA, An SJ, Li J, Wood DL, Nanda J (2018) Chemical evolution in silicon-graphite composite anodes investigated by vibrational spectroscopy. ACS Appl Mater Interfaces 10:18641–18649. https://doi.org/10.1021/acsami.8b02197
32. Cuesta N, Ramos A, Cameán I, Antuña C, García AB (2015) Hydrocolloids as binders for graphite anodes of lithium-ion batteries. Electrochim Acta 155:140–147. https://doi.org/10.1016/j.electacta.2014.12.122
33. Farooq U, Choi JH, Atif Pervez S, Yaqub A, Kim DH, Lee YJ, Saleem M, Doh CH (2014) Effect of binder and composition ratio on electrochemical performance of silicon/graphite composite Battery electrode. Mater Lett 136:254–257. https://doi.org/10.1016/j.matlet.2014.08.059
34. Hochgatterer NS, Schweiger MR, Koller S, Raimann PR, Wöhrle T, Wurm C, Winter M (2008) Silicon/graphite composite electrodes for high-capacity anodes: Influence of binder chemistry on cycling stability. Electrochem Solid-State Lett 11:A76. https://doi.org/10.1149/1.2888173
35. Doerffel D, Sharkh SA (2006) A critical review of using the Peukert equation for determining the remaining capacity of lead-acid and lithium-ion batteries. J Power Sources 155:395–400. https://doi.org/10.1016/j.jpowsour.2005.04.030
36. Wu G, Li C, Jiao D, Liu Y, Hao C, Zhang Y, Yu H, Zhang M (2016) State of charge estimation for Li-ion battery based on an improved Peukert's equation with temperature correction factor. 2016 IEEE Vehicle Power and Propulsion Conference (VPPC). IEEE, New York, pp 4–7. https://doi.org/10.1109/VPPC.2016.7791780
37. Omar N, Van den Bossche P, Coosemans T, Van Mierlo J (2013) Peukert revisited-critical appraisal and need for modification for lithium-ion batteries. Energies 6:5625–5641. https://doi.org/10.3390/en6115625
38. Zhang Y, Tang Y, Deng J, Leow WR, Xia H, Zhu Z, Lv Z, Wei J, Li W, Persson C, Malyi OI, Antonietti M, Chen X (2019) Correlating the Peukert's constant with phase composition of electrode materials in fast lithiation processes. ACS Mater Lett 1:519–525. https://doi.org/10.1021/acsmaterialslett.9b00320
39. Sung J, Kim N, Ma J, Lee JH, Joo SH, Lee T, Chae S, Yoon M, Lee Y, Hwang J, Kwak SK, Cho J (2021) Subnano-sized silicon

anode via crystal growth inhibition mechanism and its application in a prototype Battery pack. Nat Energy 6:1164–1175. https://doi.org/10.1038/s41560-021-00945-z
40. Asenbauer J, Eisenmann T, Kuenzel M, Kazzazi A, Chen Z, Bresser D (2020) The success story of graphite as a lithium-ion anode material-fundamentals, remaining challenges, and recent developments including silicon (oxide) composites, sustain. Energy Fuels 4:5387–5416. https://doi.org/10.1039/d0se00175a
41. Wetjen M, Pritzl D, Jung R, Solchenbach S, Ghadimi R, Gasteiger HA (2017) Differentiating the degradation phenomena in silicon-graphite. J Electrochem Soc 164:A2840–A2852. https://doi.org/10.1149/2.1921712jes
42. Yao KPC, Okasinski JS, Kalaga K, Almer JD, Abraham DP (2019) Operando quantification of (de)lithiation behavior of silicon–graphite blended electrodes for lithium-ion batteries. Adv Energy Mater 9:1803380. https://doi.org/10.1002/aenm.201803380
43. Artrith N, Urban A, Ceder G (2018) Constructing first-principles phase diagrams of amorphous LixSi using machine-learning-assisted sampling with an evolutionary algorithm. J Chem Phys 148:1–10. https://doi.org/10.1063/1.5017661
44. Hamzelui N, Eshetu GG, Figgemeier E (2021) Customizing active materials and polymeric binders: stern requirements to realize silicon-graphite anode based lithium-ion batteries. J Energy Storage 35:102098. https://doi.org/10.1016/j.est.2020.102098
45. Mazouzi D, Lestriez B, Roué L, Guyomard D (2009) Silicon composite electrode with high capacity and long cycle life. Electrochem Solid-State Lett 12:A215. https://doi.org/10.1149/1.3212894
46. Andersen HF, Foss CEL, Voje J, Tronstad R, Mokkelbost T, Vullum PE, Ulvestad A, Kirkengen M, Mæhlen JP (2019) Silicon-Carbon composite anodes from industrial Battery grade silicon. Sci Rep 9:1–9. https://doi.org/10.1038/s41598-019-51324-4
47. Tranchot A, Idrissi H, Thivel PX, Roué L (2016) Impact of the slurry pH on the expansion/contraction behavior of silicon/carbon/carboxymethylcellulose electrodes for Li-ion batteries. J Electrochem Soc 163:A1020–A1026. https://doi.org/10.1149/2.1071606jes
48. Kim B, Song Y (2023) Dispersion homogeneity of silicon anode slurries with various binders for Li-ion Battery anode coating. Rheol Process Polym Mater 15:1152. https://doi.org/10.3390/polym15051152
49. Gao H, Wu Q, Hu Y, Zheng JP, Amine K, Chen Z (2018) Revealing the rate-limiting Li-ion diffusion pathway in ultrathick electrodes for Li-ion batteries. J Phys Chem Lett 9:5100–5104. https://doi.org/10.1021/acs.jpclett.8b02229
50. Nöske M, Breitung-Faes S, Kwade A (2019) Electrostatic stabilization and characterization of fine ground silicon particles in ethanol. Silicon 11:3001–3010. https://doi.org/10.1007/s12633-019-0089-0
51. Zhu T, Hu Q, Yan G, Wang J, Wang Z, Guo H, Li X, Peng W (2019) Manipulating the composition and structure of solid electrolyte interphase at graphite anode by adjusting the formation condition. Energy Technol 7:1–9. https://doi.org/10.1002/ente.201900273
52. Guo J, Sun A, Chen X, Wang C, Manivannan A (2011) Cyclability study of silicon-carbon composite anodes for lithium-ion batteries using electrochemical impedance spectroscopy. Electrochim Acta 56:3981–3987. https://doi.org/10.1016/j.electacta.2011.02.014



## Authors and Affiliations

**Alper Güneren[1,2] · Ahmed A. Nada[2,3,4] · Alena Opálková Šišková[4] · Katarína Mosnáčková[2,4] · Angela Kleinová[4] · Jaroslav Mosnáček[2,4] · Zoltán Lenčéš[1]**

✉ Alper Güneren
uachalgu@savba.sk

Ahmed A. Nada
ahmed_nada@hotmail.com

Alena Opálková Šišková
alena.siskova@savba.sk

Katarína Mosnáčková
katarina.mosnackova@savba.sk

Angela Kleinová
angela.kleinova@savba.sk

Jaroslav Mosnáček
upolmosj@savba.sk

Zoltán Lenčéš
zoltan.lences@savba.sk

[1] Institute of Inorganic Chemistry, Slovak Academy of Sciences, 84536 Bratislava, Slovakia

[2] Centre for Advanced Materials Application (CEMEA), Slovak Academy of Sciences, 84511 Bratislava, Slovakia

[3] Pretreatment and Finishing of Cellulose Based Textiles Department, National Research Centre, Giza 12622, Egypt

[4] Polymer Institute, Slovak Academy of Sciences, 84541 Bratislava, Slovakia